

# Weak coupling cavity quantum electrodynamics of monolayer lead sulfide nanocrystals in silicon photonic crystal cavities at the near-infrared

R. Bose\*, J. Gao, J. F. McMillan, F. W. Sun, X. Yang, C. J. Chen, and C. W. Wong\*

Optical Nanostructures Laboratory, Center for Integrated Science and Engineering, Solid-state Science and Engineering, and Mechanical Engineering, Columbia University, New York, NY 10027

\*rb2261@columbia.edu; cww2104@columbia.edu

Abstract:

A detailed experimental analysis of weak coupling between monolayer lead sulfide nanocrystals and silicon photonic crystal nanocavities is presented at room as well as cryogenic temperatures at the near-infrared. It is found that surface perturbations induced by the random quantum dot integration plays a significant effect on the cavity field mode. A reduced *quality factor* is observed as a result of quantum dot integration, but strong polarization extinction is still observed. Different enhancements are also observed from dots coupled to photonic crystals with different design parameters and are explained through the nature of corresponding planar wavevector components of the cavity mode dispersion. Finally the coupling of dots to multistep heterostructure cavities is analyzed at room and cryogenic temperatures. Intensity-saturation effects of QDs coupled to the heterostructure mode at 4K are studied with the results suggesting a rate enhancement for coupled dots compared to dots off-resonance. The studies presented here have important implications for silicon-based near-infrared single photon sources.

Cavity quantum electrodynamics (cQED) experiments in the near-infrared are strongly motivated by the need for an efficient on-demand single-photon source that has importance in many quantum cryptography and quantum information processing applications. Charged carriers, or excitons, in single quantum dots (QD) can be excited in a controllable way to inhibit multi-photon emission, enabling a single-photon source [1,

2]. Coupling of the single QD to high-quality localized modes in photonic crystals (PhCs) through accurate positional and spectral alignment permits strong modifications to the exciton radiative recombination processes such that photons can be extracted before exciton dephasing occurs, allowing for photon indistinguishability [1]. In solid-state QD applications, a strong emphasis is therefore placed on QD engineering for optimized spatial [3] and spectral [4] overlap, or with various material systems [5], with resonant mesoscopic cavity modes. Chip-scale spatial positioning and spectral tuning in an array can allow for scalable quantum information processing elements [6, 7].

Compared with other solid-state technologies, silicon-based PhCs have shown remarkable achievements in high-quality devices arising from the well-developed processing techniques. Novel optical phenomena have already been demonstrated and highly elaborate optical networks are envisioned on-chip, and the possibility of an integrated single-photon source is of great promise. In developing a silicon-based cQED material system however, a problem arises immediately due to the lack of a non-invasive way to address the cavity modes. Colloidal QDs from IV-VI materials, such as lead sulfide (PbS) and lead selenide (PbSe), can be integrated on the device surface and positioned accurately using lithography or chemical techniques. Lead-salt QDs have shown great promise in important applications when used in large ensembles [8,9], but have not been studied extensively as single, isolated emitters. Colloidal PbS QD, like CdSe QD [10] demonstrate rapid Auger recombination, allowing for multi-exciton suppression and antibunching, which is important for single-photon applications. However, experiments involving PbS QDs are limited through a lack of knowledge of the complete energy structure of a single QD. Measurements on single QDs have revealed an

unusually large bandwidth ( $\sim 80$  nm) for the ground state exciton at 900 nm [11], explained most accurately by a non-degeneracy of the 64 possible  $1S_e$ - $1S_h$  transitions that arise from the eight-fold degeneracy of the extrema at the L-point of the Brillouin zone [12]. Distinguishing these non-degenerate exciton states in real experiments may prove to be a considerable challenge. Coupling of QDs to PhC nanocavities may provide considerable insight into the quantum states of the nanoparticles.

In weak coupling measurements of lead sulfide dots coupled to silicon PhC cavities between room temperature and 4K, the Purcell effect [13] is generally invoked to explain the observed enhancements of the QD emission at the perceived peak of the cavity resonance. The expression for the Purcell Factor is:

$$F_p = \frac{3\lambda^3}{4\pi^2 n^3} \frac{Q_c}{V_{eff}} \quad (1)$$

The enhancement of spontaneous emission rates due to the PhC environment is then given, for a single emitter, by [14]:

$$E = \frac{\Gamma_{cav}}{\Gamma_o} = F_{CAV} + F_L = F_p \times \left( \frac{\omega}{\gamma_{cav} + \gamma_e} \right) \times \frac{[(\gamma_{cav} + \gamma_e)/2]^2}{(\omega_{cav} - \omega_e)^2 + [(\gamma_{cav} + \gamma_e)/2]^2} \times \left( \frac{\bar{E}(\bar{r}) \cdot \bar{\mu}}{|\bar{E}_{max}| |\bar{\mu}|} \right)^2 \times \eta^2 + F_L \quad (2)$$

where in the final expression  $\gamma_e$  and  $\gamma_{cav}$  denote QD and cavity lifetimes,  $\omega_e$  and  $\omega_{cav}$  are the emitter and cavity frequencies, the fourth term accounts for spatial coupling, and  $\eta^2$  accounts for the polarization mismatch.  $F_L$  accounts for the base spontaneous emission rate from coupling to photonic crystal Bloch modes without the cavity, and is related to

the spontaneous emission coupling factor  $\beta$  through  $\beta = F_{CAV} / (F_{CAV} + F_L)$  [15]. The enhancement of radiation observed at the cavity wavelength in experiments is a result of both the cavity directionality and the QD enhanced spontaneous emission rate according to equation (2).

PbS QDs exhibit long radiative recombination lifetimes due to strong dielectric screening effects. For dots in solution, the measured lifetimes are around 1  $\mu$ s [16]. In closely packed films, the observed lifetimes range between 80 to 200 ns at room temperature due to a changed local field factor [12] as well as possibly reduced quantum efficiency, with a trend towards increasing lifetimes at lower temperatures as we have observed [16]. These numbers agree with theoretical predictions in literature. A direct consequence of long lifetimes (compared to InAs  $\sim$ 1 ns), is that fewer photons are emitted per second per dot. As a result, we cannot presently detect emission from single dots. This necessitates operation of ensemble QD-PhC devices in cQED experiments. However, the non-degeneracy of the lowest exciton state implies that single dot operation does not necessarily involve a single exciton state. In most experiments involving cQED with PbS QDs [17-20], large ensembles of closely-packed QDs are used due to issues with low signal levels. In our experiments reported here, we use a very sparse concentration of dots (between 100-1000 per  $\mu\text{m}^2$  in a *single* layer,  $< 6$  nm thickness) to allow for stronger coupling and to prevent any radiative or non-radiative inter-dot interactions. As we see later, the low concentration of QD also allows us to study saturation effects for coupled and uncoupled dots. We are able to observe results using high-quality near-infrared (gated) detectors and optical components, and by sacrificing spectral resolution in order to achieve higher throughput in the monochromator.

Devices are designed using standard FDTD techniques [21]. The PhCs exhibit a triangular lattice that supports a TE band gap for propagating modes [22]. By removing a set of 3 linear holes, a defect is formed [23] where high- $Q$  modes can be confined for cQED measurements (fig 1a). In a PhC, planar confinement is afforded by the 2D periodic lattice of the PhC, whereas vertical confinement occurs via total internal reflection. At the silicon-air interface, in-plane wave-vectors  $k_{\parallel}$  that satisfy  $|k_{\parallel}| < 2\pi/\lambda$  can escape in the vertical direction, thereby reducing  $Q$ , whereas wave-vector components that do not satisfy this condition are confined in the slab region. A smoothing of the cavity wavefunction envelope at the cavity edges results in reduced  $k_{\parallel}$  components within the light cone [24, 25, 26]. For silicon-on-insulator (SOI) devices in the first part of the experiments, the parameters are  $a = 420$  nm,  $r = 0.319a$ ,  $t_{Si} = 250$  nm. Either one (“ $s1$ ”, figure 1c) or three (“ $s123$ ”, figure 1d) holes on each side of the cavity-edge are detuned from their original position for initial  $Q$ -optimization using the abovementioned techniques [26]. The devices are fabricated through optimized deep-UV lithography and etched into the silicon film. All devices have on-board waveguides that enable device characterization prior to QD integration. PbS QDs are synthesized using standard methods [27, 28], dispersed in chloroform, and have a center wavelength  $\lambda_0$  of 1490 nm with a spectral width  $\Delta\lambda$  of  $\sim 150$  nm at room temperature. The quantum dots are obtained from Evident Technologies, and are integrated directly through a spin-coating procedure that results in a single layer of dots on the device surface with various areal densities.

In the experiments, a HeNe laser (average pump power of 1 to 10 mW) or a 980 nm diode laser (1 to 60 mW average power) is used to non-resonantly pump the QDs on the

surface of the PhC defect using a 100× objective lens. The emission is collected through the same lens and dispersed using a 32-cm monochromator for detection by a liquid nitrogen-cooled germanium detector. For confocal measurements, the collected emission is focused on an optical fiber and detected using a gated InGaAs/InP avalanche photodiode from Princeton Lightwave with appropriate control electronics, bias and afterpulse suppression.

Figure 1e shows experimental results of the QDs on a *L3* PhC cavity, showing emission enhancements for silicon-on-insulator devices designed for the same emission wavelengths (~1550 nm), but different *Q*s. After QD integration, the cavity *Q* (originally ~1500) drops by a factor of 30 to ~50, and the resonance blue-shifts by ~-50 nm. By integrating random QDs (5.5 nm diameter) at the silicon-air interface, the total internal reflection conditions within the PhC are strongly modified for the in-plane wave-vectors, resulting in a re-shaping of the in-plane field component  $E_x(x,y)$  at the slab surface as well as a modified *Q*. The *s1* and *s123* devices yield similar *Q* due to the surface QD. However, the observed mode shows linear TE polarization dependence, as predicted by FDTD simulations for the unperturbed devices. For TE polarization, the coupled QDs exhibit 5-fold enhancements over the background (blue curve, figure 1e). Although the QDs are randomly integrated due to the spin-coating, it is surprising to see that the resonances remain very similar ( $\pm 10$ nm, figure 1e) across several devices on the same chip.

After these initial measurements, we further reduced the number of QDs on the sample surface. Figure 2a shows the minimum number of dots (~100) that we are able to presently measure in our setup, after enhancements from the cavity. In figure 2b, the

polarization dependence of the observed cavity mode is shown for this device. Confocal scans of the devices (figure 2c) confirm that the emission originates from the cavity ( $\sim 20$  counts/sec at 2 MHz, signal to noise 10:1). From the measured cavity  $Q$  ( $\sim 75$ ), the estimated maximum  $P_F$  enhancement for this mode is 5, using equation (1), although this number could be considerably different due to a modified mode volume after QD integration. Due to the mode-confinement profiles and the resulting enhancements, the resonance is clearly observed over the background QD emission with an overall 8-fold enhancement for TE-polarized emission, and a polarization extinction ( $I_{90}/I_0$ ) of 10. We attribute this enhancement to a combined effect of faster radiative recombination rates as well as improved collection efficiency at the high N.A (0.9) objective lens for dots coupled to the cavity mode. Averaging the calculated cavity field profiles at slab center (over a  $1 \mu\text{m}^2$  cavity mode area from the top) gives an average value of 0.3 for the spatial component  $\left[ \overline{E(r)} \cdot \overline{\mu} / \left| \overline{E_{\text{max}}} \right| \left| \overline{\mu} \right| \right]^2$  of the enhancement equation (2). After QD integration on the device surface, the z-component of the electric field is expected to be modified considerably due to a change in refractive index, possibly allowing for a high value of the spatial enhancement factor even at the slab surface. With high spectral overlap due to the availability of several quantum dots with possibly large emission linewidths, it is then possible to observe coupled QD emission over the background. It should be noted from equation (2) that it evidently seems possible to observe the cavity mode over the background even without the Purcell effect, if  $F_L \sim 1 \gg F_{CAV}$ . However, the resulting  $\beta$ -factor in this case approaches  $F_{CAV}$  which means that a very small percentage of quantum dots emit into the mode, and imposes an unreasonable requirement for collection efficiency for these photons to explain the observed results. For the high-quality devices

presented in this work, we further expect a strong suppression of photonic crystal Bloch modes such that the value of  $F_L \sim 0.1$ . The complex exciton energy structure of PbS probably results in a more complicated model for cQED. In a later section, we study the power dependence of QD saturation for an experimental attempt to experimentally isolate contributions due to Purcell enhancements. We note that, on monitoring the QD intensity at the resonance of the emission over a time of many minutes, we do not observe any evidence of blinking, suggesting that several quantum dots still emit into the mode, although the QD concentration is very low.

The perturbation and resulting changes in the vertical field profile allow QDs to couple spatially with the cavity mode. To further highlight this effect and enable an in-depth analysis of the rate-enhancement equation (2), we fabricated devices with different  $r/a$  ratios and observed the coupling behavior of PbS dots positioned above the cavities as a function of cavity-mode resonance wavelengths. The devices here are air-bridged allowing for high initial  $Q$ -factors ( $\sim 40\,000$ ). After integration of the QDs, the  $Q$  drops considerably, with the sharpest observed features yielding  $Q$ s of  $\sim 200$ - $500$ , corresponding to a maximum  $P_F$  of about 10 to 25 using (1), assuming that the effective volume is not altered considerably by the QD integration. The results in figure 3b show coupled devices for  $r$  of  $0.2755a$ ,  $0.29a$ , and  $0.3045a$  for a value of  $a = 420$  nm, and a slab thickness of  $\sim 220$  nm. For basic comparison, we compute the theoretical resonances, calculated using FDTD. The different values of  $r/a$  also result in a shift in the bandgaps that are observed in FDTD simulations (figure 3a). Theoretically, the bandgap as well as the defect mode red-shifts with decreasing filling factors. We map out the cavity mode for these values of  $r$ , and observe resonances that are consistent with the theoretical predictions, and



conclude that the observed modes are likely derived as perturbations of the original field profiles. We consistently observe the lowest enhancements from the mode centered at 1500 nm, although this mode exhibits the highest  $Q$ -factors. This difference is not explained through different QD availability on resonance, and we thus infer that this is due to the relative position of the mode in the PhC bandgap that allows for a smaller component of the electric field at the slab surface, resulting in a smaller interaction with surface QDs, as well as smaller sensitivity of the  $Q$  to surface perturbations. Here again, the results imply a contribution of the spatial enhancement component of  $F_{CAV}$ . As a further note, devices fabricated for  $r=0.261a$  did not show QD coupling in the measurements but are characterized using the waveguide before QD integration with a resonance  $\lambda_0$  of  $\sim 1550$  nm. The emission enhancement contrast over the background ranges between 1.5 and 4 for mixed-polarization emission.

We notice that the device  $Q$  is not improved considerably by reducing the number of surface dots, suggesting that a small perturbation is sufficient to cause the modes to be leaky in the  $z$ -direction for the  $L3$  PhC mode. Higher- $Q$  modes are more sensitive to issues such as surface roughness, and it is not altogether surprising to see a  $200\times$  reduction in the  $Q$  for the air-bridged devices. Due to the large bandwidth of single QDs at room temperature, spectral alignment to the cavity is easily obtained. The experiments are highly repeatable, and similar concentrations of dots on the surface result in observed modes with resonance deviations of less than 10 nm. For enhanced coupling to higher- $Q$  modes, cavities can be designed with higher field intensities in the “air” regions, for example, using coupled  $L1$  cavities, and by envisioning novel chemical and physical techniques for QD integration. The  $L3$  cavities do not exhibit far-field profiles ideally

suited for normal incident pump and collection experiments, but are useful in our case to highlight contributions due to the Purcell Effect in the measurements.

Exciton states at room temperature are homogeneously broadened due to coupling to lattice vibrations, or phonons. At low temperature, coupling to phonons is greatly reduced, and QD linewidths are shorter, resulting in longer dephasing times that are well-suited for single-photon source-applications. To see the change in QD-cavity coupling as a function of temperature, we consider the multistep-heterostructure cavity (fig 4a), as suggested in [29]. In these devices, photon confinement is achieved through a mode-gap effect induced by a changing lattice parameter to create a potential well. The mode profiles are similar to the  $L3$  modes used above [29]. In these experiments, we use silicon-on-oxide devices that support much lower  $Q$  ( $\sim 5000$ ), allowing easier QD integration processes. We observe shifted resonances for the multistep heterostructure cavity for different values of the filling factor  $r/a$  (figure 4b). To the best of our knowledge, this is the first demonstration of QDs coupled to silicon-based multi-step PhC structures. The  $L6$  cavity region does not possess a high- $Q$  due to symmetry requirements, but is designed for optimal mode-excitation in planar measurements as an example.

Due to additional losses at the cryostat, we use a higher concentration of dots (figure 4c and d) when cooled to low temperatures. We observe a strong red-shift in the ensemble QD emission (120 nm) as we tune the temperature from 295K to 4K (figure 4e), with maximum emission observed at 160K. The latter behavior is most likely caused by the ambient environment inside the cryostat at low temperature. The shifts in PL peak emission with changing temperature is not linear over the range of 4 to 295K. Over the

same temperature range, the shift in the cavity resonance is blue-shifted by only 20 nm (0.06 nm/K), due to the refractive index change of silicon (Si thermo-optic constant  $1.86 \times 10^{-4} K^{-1}$ ). In ensemble measurements, QD linewidths are reduced from 150 nm at 295K to 80 nm at 4 K, suggesting a reduction in the homogeneous linewidth. This behavior results in a lower probability of spectral alignment for sparse QDs on the sample surface, and only a few devices can be characterized, compared to 295K where resonances are observed from every device.

When coupled to cavities, QD generally exhibit higher saturation thresholds due to a lower probability of exciton occupation at any time arising from an increased spontaneous emission rate. In the absence of a direct lifetime measurement, the onset of saturation for coupled and uncoupled dots may be used in continuous wave (cw) measurements to approximate the Purcell effect as a ratio of the saturation powers [30]. In PbS QD, due to the large number of excitons needed for transparency as well as rapid Auger recombination, very high intensity excitation is traditionally required to saturate QD emission when studied in large ensembles [31]. However, the sparse QDs used in this study allow us to study saturation effects of the quantum dots at moderate excitation levels. Power-dependent measurements of the heterostructure mode are shown in figure 5a over the experimentally-limited range of 7.5 to 60 mW averaged power from a 980 nm diode laser. We do not observe any broadening of the cavity spectrum (reduced  $Q$  factor) due to the laser source over this range. Since the experiments are performed at 4K, nonradiative mechanisms are expected to be low [32, 33]. In figure 5b, we plot the response of QD at- and near the cavity resonance, as well as uncoupled QD, as a function of the input excitation power. The data are derived from the graphs in figure 5a, after a

mathematical smoothing step is used to reduce experimental noise. By averaging the intensity as a function of power for *all* dots on- and off-resonance, we clearly see a difference in the power-dependent behavior of these QDs that cannot be explained through geometric effects. We plot the power-dependence of uncoupled dots at the peak of the background PbS spectrum (1600 nm at 4K) as well as at 1450 nm to show that the results are independent of QD number, and to exclude multiexciton interactions alone as being a possible cause of these observations. These results suggest operation in the saturation region for QDs that are not coupled to the mode resonance and an absence of the saturation onset over this power range for dots emitting in the mode resonance, and provide strong evidence that state-filling effects play a role in the observed enhancements. We deduce an ensemble Purcell factor of more than 1 from these experiments. For a strongly suppressed value of  $F_L=0.1$ , a beta factor of 90% can then be approximated for this cavity-QD system, along with a geometric coupling enhancement of  $\sim 4$ . Future studies will be conducted to accurately quantify the saturation powers for on- and off-resonance dots.

In conclusion, we present a detailed analysis of weak coupling for monolayer PbS QD coupled to silicon PhC cavities. The results make a strong case for Purcell-effect enhancements for QDs coupled to the cavity modes. By designing PhC with different parameters, as well as by temperature-tuning the dots, we observe different degrees of coupling of QD and the cavity mode field in spectral measurements. We observe high polarization extinction ratios for  $L3$  SOI PhC cavities. For a very small concentration of QD, we do not observe any blinking characteristics, which presently rules out single QD operation. The experiments are highly repeatable, and the QD can be washed out using

solvents and reintegrated allowing for large overall device performance lifetime. The PhC response to the randomly integrated QDs is highly repeatable. We further perform QD exciton saturation effects at 4K in SOI heterostructure cavities to quantify the role of Purcell enhancements in the observed results. The results clearly exhibit different state-filling effects for on- and off-resonance dots. We also suggest cavity design configurations for enhanced coupling of QD and the PhC modes that may yield higher quality systems for future work. We believe that the work holds promise for chip-scale cQED and single photon sources in the next generation of silicon optical networks.

#### ACKNOWLEDGEMENT

The authors acknowledge helpful discussions with S. Jockusch, N. Turro, and R. L. Williams, and lithography fabrication from M. Yu and D.-L. Kwong at the Institute of Microelectronics in Singapore. The authors acknowledge funding support from the DARPA, the New York State Office of Science, Technology and Academic Research, and the National Science Foundation CAREER Award.

## References

- [1] C. Santori, D. Fattal, J. Vučković, G. S. Solomon, Y. Yamamoto, *Nature* **419**, 594 (2002); M. Pelton, C. Santori, J. Vučković, B. Zhang, G. S. Solomon, J. Plant and Y. Yamamoto, *Phys. Rev. Lett.* **29**, 233602 (2002)
- [2] See for example: W.-H. Chang, W.-Y. Chen, H.-S. Chang, T.-P. Hsieh, J.-I. Chyi, and T.-M. Hsu, *Phys. Rev. Lett.* **96**, 117401 (2006); D. Press, S. Götzinger, S. Reitzenstein, C. Hofmann, A. Löffler, M. Kamp, A. Forchel, and Y. Yamamoto, *Phys. Rev. Lett.* **98**, 117402 (2007); S. Strauf, N. G. Stoltz, M. T. Rakher, L. A. Coldren, P. M. Petroff, and D. Bouwmeester, *Nature Photonics* **1**, 704 (2007); C. Santori, D. Fattal, J. Vuckovic, G. S. Solomon, Y. Yamamoto, *New. J. Phys.* **6**, 89 (2004); A. Shields, *Nature Photonics* **1**, 215 (2007)
- [3] See for example: B. L. Liang, P. S. Wong, N. Nuntawong, A. R. Albrecht, J. Tatebayashi, T. J. Rotter, G. Balakrishnan, and D. L. Huffaker, *Appl. Phys. Lett.* **91**, 243106 (2007); P. Chen, A. Chen, S. J. Chua, and J. N. Tan, *Adv. Mat.* **19**, 1707 (2007); A. Badolato, K. Hennessy, M. Atatüre, J. Dreiser, E. Hu, P. M. Petroff, and A. Imamoglu, *Science* **308**, 1158 (2005); S. Frederick, D. Dalacu, P. J. Poole, J. Lapointe, G. C. Aers, R. L. Williams, *Phys. Stat. Sol. (c)* **3**, 3685 (2006); K. Hennessy, A. Badolato, P. M. Petroff, E. Hu, *Photonics and Nanostructures- Fundamentals and Applications* **2**, 65 (2004)
- [4] See for example: K. Srinivasan and O. Painter, *Nature* **450**, 862 (2007); D. Englund, A. Faraon, I. Fushman, N. Stoltz, P. Petroff, J. Vuckovic, *Nature* **450**, 857 (2007); T. Yoshie, A. Scherer, J. Hendrickson, G. Khitrova, H. M. Gibbs, G. Rupper, C. Ell, O. B. Shchekin, D. G. Deppe, *Nature* **432**, 200 (2004); J. P. Reithmaier, G. Sek, A. Löffler, C.

Hofmann, S. Kuhn, S. Reitzenstein, L. V. Keldysh, V. D. Kulakovskii, T. L. Reinecke, A. Forchel, *Nature* **432**, 197 (2004)

[5] See for example: S. Kako, C. Santori, K. Hoshino, S. Gotzinger, Y. Yamamoto, Y. Arakawa, *Nature Mat.* **5**, 887 (2006); M. W. McCutcheon and M. Loncar, Design of a silicon nitride photonic crystal nanocavity with a Quality factor of one million for coupling to a diamond nanocrystal, *Optics Express* **16**, 19136 (2008); K.-M.C. Fu, C. Santori, P.E. Barclay, I. Aharonovich, S. Praver, N. Meyer, A. M. Holm, R.G. Beausoleil, <http://arxiv.org/abs/0811.0328>

[6] See for example: H. Mabuchi and A. C. Doherty, *Science* **298**, 1372 (2002); S. J. Devitt, W. J. Munro and K. Nemoto, arXiv:0810.2444 (2008); A. M. Stephens, Z. W. Evans, S. J. Devitt, A. D. Greentree, A. G. Fowler, W. J. Munro, J. L. O'Brien, K. Nemoto and L.C.L. Hollenberg, *Phys. Rev. A* **78**, 032318 (2008); D. Bouwmeester, A. K. Ekert, and A. Zeilinger, *The Physics of Quantum Information*, Springer, Berlin, 2000.

[7] Y.-F. Xiao, J. Gao, X.-B. Zou, J. F. McMillan, X. Yang, Y.-L. Chen, Z.-F. Han, G.-C. Guo, and C. W. Wong, *New. J. Phys.*, (to appear), 2008; J. Gao, F. Sun, and C. W. Wong, *Appl. Phys. Lett.* **93**, 151108 (2008).

[8] S. Hoogland, V. Sukhovatkin, I. Howard, S. Cauchi, L. Levina, E. H. Sargent, *Opt. Exp.* **14**, 3273 (2006).

[9] R. D. Schaller, V. I. Klimov, *Phys. Rev. Lett.* **92**, 186601 (2004)

[10] X. Brokmann, G. Messin, P. Desbiolles, E. Giaocobino, M. Dahan, J. P. Hermier, *N. Jour. Phys.* **6**, 99 (2004); P. Michler, A. Imamoglu, M. D. Mason, P. J. Carson, G. F. Strouse and S. K. Buratto, *Nature* **406**, 968 (2000).

- [11] J. J. Peterson and T. D. Krauss, *Nano Lett.* **6**, 510 (2006)
- [12] G. Allan, C. Delerue, *Phys. Rev. B* **70**, 245321 (2004)
- [13] E. M Purcell, *Phys. Rev.* **69**, 681 (1946); also see for example: P. Lodahl et al. *Nature* **430**, 654 (2004), S. Noda et al. *Nature Photonics* **1**, 449 (2007)
- [14] L. C. Andreani, G. Panzarini, and J.-M. Gérard, *Phys. Rev. B* **60**, 13276 (1999) ; H. Y. Ryu and M. Notomi, *Opt. Lett.* **28**, 2390 (2003)
- [15] R. Oulton, B. D. Jones, S. Lam, A. R. A. Chalcraft, D. Szymanski, D. O'Brien, T. F. Krauss, D. Sanvitto, A. M. Fox, D. M. Whittaker, M. Hopkinson, M. S. Skolnick, *Opt. Exp.* **15**, 17221 (2007)
- [16] R. Bose, J. F. McMillan, J. Gao, C. Chen, K. M. Rickey, D.V. Talapin, C. V. Murray, C.W. Wong, *Nano Lett.* **8**, 2006 (2008)
- [17] R. Bose, X. Yang, R. Chatterjee, J. Gao, C.W. Wong, *Appl. Phys. Lett.* **90**, 111117 (2007); R. Bose, D. V. Talapin, X. Yang, R. J. Harniman, P. T. Nguyen, and C. W. Wong, *Proc. SPIE* **6005**, 600509 (2005)
- [18] I. Fushman, D. Englund, and J. Vučković, *Appl. Phys. Lett.* **87**, 241102 (2005)
- [19] J. Yang, J. Heo, T. Zhu, J. Xu, J. Topolancik, F. Vollmer, R. Ilic, P. Bhattacharya, *Appl. Phys. Lett.* **92**, 261110 (2008)
- [20] Z. Wu, Z. Mi, P. Bhattacharya, T. Zhu, J. Xu, *Appl. Phys. Lett.* **90**, 171105 (2007)
- [21] A. Farjadpour, D. Roundy, A. Rodriguez, M. Ibanescu, P. Bermel, J. D. Joannopoulos, S. G. Johnson, and G. Burr, *Opt. Lett.* **31**, 2972 (2006)



- [22] R. Chatterjee, N. C. Panoiu, K. Liu, Z. Dios, M. B. Yu, M. T. Doan, L. J. Kaufman, R. M. Osgood, and C. W. Wong, *Phys. Rev. Lett.* **100**, 187401 (2008)
- [23] X. Yang, C. Husko, M. Yu, D.-L. Kwong, and C. W. Wong, *Appl. Phys. Lett.* **91**, 051113 (2007).
- [24] Y. Akahane, T. Asano, B. Song, and S. Noda, *Opt. Exp.* **13**, 1202 (2005)
- [25] K. Srinivasan and O. Painter, *Optics Express* **10**, 670 (2002)
- [26] Y. Akahane, T. Asano, B.-S. Song, and S. Noda, *Nature* **425**, 944 (2003)].
- [27] C. B. Murray, S. Sun, W. Gaschler, H. Doyle, T. A. Betley, C. R. Kagan, *IBM J. Res. & Dev.* **45**, 47 (2001)
- [28] M. A. Hines, G. D. Scholes, *Adv. Mater.* **15**, 1844 (2003)
- [29] B-S. Song, S. Noda, T. Asano, Y. Akahane, *Nature Mat.* **4**, 207 (2005)
- [30] J. M. Gérard, B. Gayral, *J. Lightwave Tech.* **17**, 2089 (1999)
- [31] Sjoerd Hoogland; personal communication
- [32] M. Makarova, V. Sih, J. Warga, R. Li, L. Dal Negro, J. Vuckovic, *Appl. Phys. Lett.* **92**, 161107 (2008).
- [33] S. Iwamoto, J. Tatebayashi, T. Fukuda, T. Nakaoka, S. Ishida, Y. Arakawa, *Jap. Jour. Appl. Phys.* **44**, 2579 (2005)

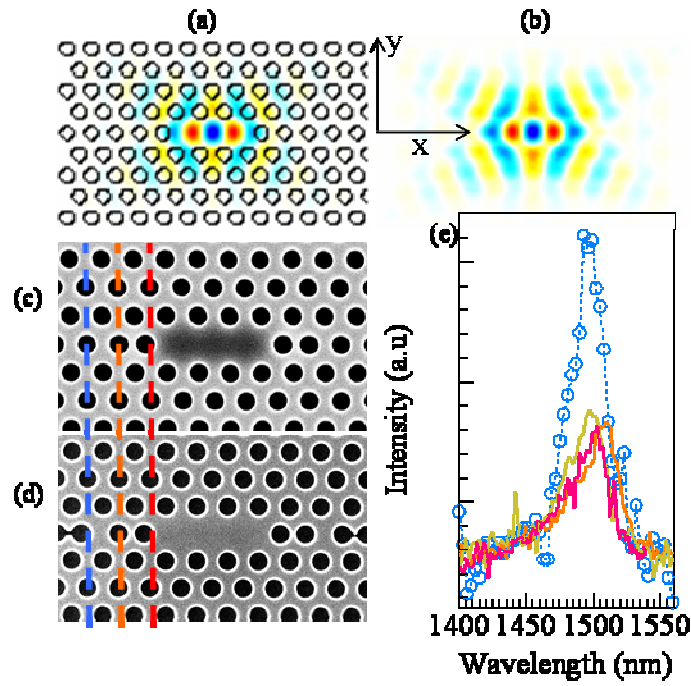


Figure 1: (a) Typical mode profile for unoptimized L3 nanocavity defect mode at slab center as well as slab-surface (b). (c and d) Scanning electron micrographs of fabricated s1 (c, edge holes shifted  $0.15a$ ) and s123 (3 edge holes shifted by  $0.176a$ ,  $0.024a$  and  $0.176a$  respectively, on both sides of cavity) devices.  $a=420$  nm. Experimentally observed defect modes for various cavities on the same-chip (SOI), designed with various detunings of the edge-holes at the same resonance wavelength, as shown in Figure 1c and d. Dotted-blue curve shows the polarization dependence of the cavity mode.

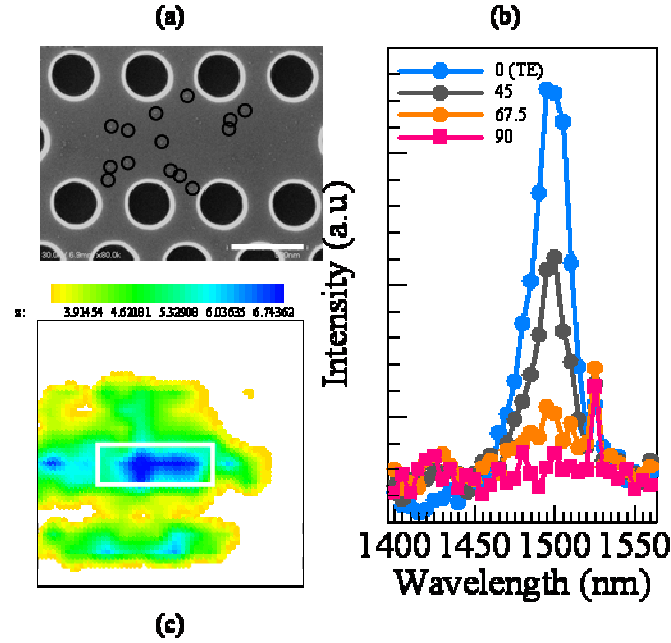


Figure 2: (a) Minimum number of dots presently measured by the Ge detector. Scale bar: 500 nm. Circles show position of single dots. (b) L3 cavity mode observed for the device shown in (a), along with the polarization extinction. The additional feature at  $\sim 1530$  nm in (b) is due to strong reflections from the laser as a result of sparse QD. (c) Confocal scan shows that the emission max occurs at the cavity. The white box represents the approximate cavity region.

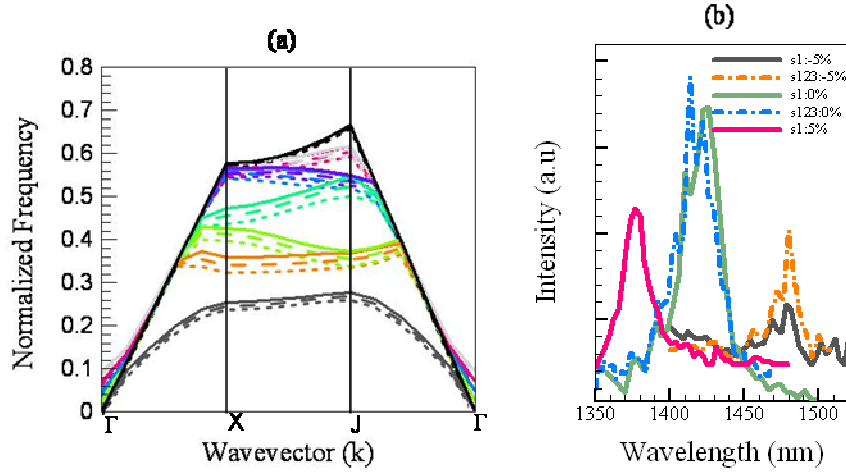


Figure 3: (a) Calculated TE bandstructure of silicon air bridged PhCs,  $r=0.29a$  (0%, dashed line),  $r=0.3045a$  (+5%, solid line),  $r=.276a$  (-5%, dotted line),  $t= 0.52a$ . The vertical axis shows the normalized frequency in  $2\pi c/a$  units. (b) Experimental modes observed for various filling factors for five different L3 cavities.  $s1$  and  $s123$  denote edge hole detunings of 1- or 3-holes on each side. The defect mode at 1500 nm typically shows lower enhancements ( $s123$  -5% is rescaled for distinction). The cavity mode corresponding to a design of  $r=0.261a$  is not observed in the coupling measurements.

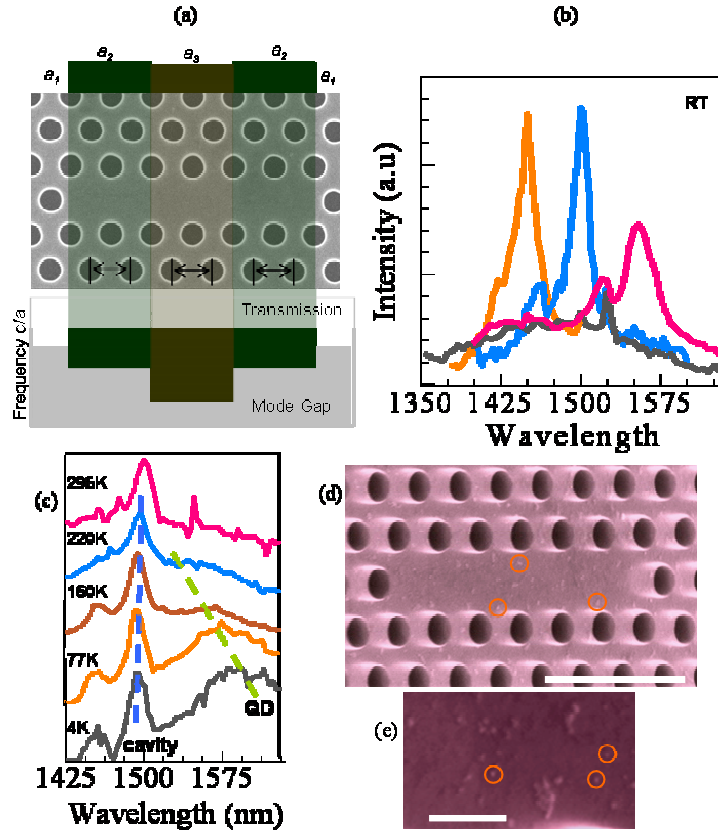


Figure 4: (a) Fabricated multi-step heterostructure PhC cavity.  $a_1=410$  nm,  $a_2=415$  nm,  $a_3=420$  nm. The mode is confined in the region of the 6 missing holes. (b) Experimentally observed modes for various values of the radius  $r$  of air holes (from left to right: 130 nm, 124 nm, 118 nm), as well as the background PL emission of the QDs. (c) Temperature dependent measurements (bottom to top: 4K, 77K, 160K, 220K and 295K) of a single mode showing cavity and QD ensemble spectral shifts with temperature, as well as the mode-gap defect mode-shift. In nearly all spectral measurements, we observe an additional peak to the left of the main peak. (d) and (e) Angled SEM of QD positioned on the surface of the heterostructure PhC cavity mode-confinement region. Orange circles show positions of a few dots. Scale bar represent  $1\text{ }\mu\text{m}$  in (d) and 100 nm in (e)

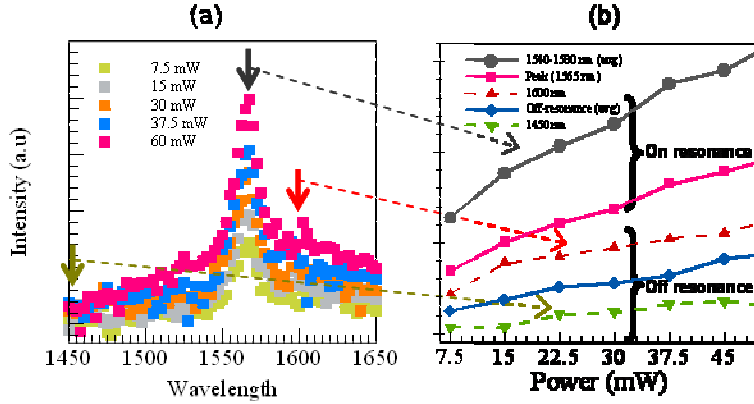


Figure 5: (a) Power dependence of the PbS PL spectrum at 4K when coupled to the multistep heterostructure mode. No line broadening is observed for the heterostructure mode ( $r=118$  nm) over a power range of 7.5 to 60 mW, measured before the objective lens. (b) Analysis of the power response of QDs on- and off-resonance shows a discernable difference. The increasing contrast of the cavity mode with respect to the background suggests a higher power threshold for saturation of emission from coupled dots compared to uncoupled dots due to an increased spontaneous emission rate. QD intensities are plotted at the peak of cavity mode, averaged over the resonance-spectrum, as well as averaged off-resonance. Further, QDs emitting at 1450 nm and 1600 nm are plotted to show that the results are independent of QD availability.